Desalination and Water Treatment
www.deswater.com

doi: 10.5004/dwt.2023.30114

315 (2023) 96–110
December

Study of acid treatment effect of a natural red clay onto physico-chemical and adsorption properties

Hassan Ouallal[a,*], Mohammed Chrachmy[a], Mohamed Azrour[a], Mahdi Lechheb[a], Abderrazek El-Kordy[b], Younes Dehmani[c], Hammou Moussout[d], Azdouz M'barek[a]

[a]*Materials Sciences for Energy and Sustainable Development Team, Department of Chemistry, Faculty of Sciences and Techniques, Moulay Ismail University, Errachidia, Morocco, emails: hassanouallalaghbalou@gmail.com (H. Ouallal), chrachmy@gmail.com (M. Chrachmy), m.azrour@fste.umi.ac.ma (M. Azrour), m.lechheb@edu.umi.ac.ma (M. Lechheb), m_azdouz@hotmail.com (A. M'barek)*
[b]*Materials, Membranes and Processes of Separation, Department of Chemistry, Faculty of Sciences, Moulay Ismaïl University, PB 11201, Zitoune, Meknes, Morocco, email: abderrazekelkordy@gmail.com*
[c]*Laboratory of Physic-Chemistry Materials, Department of Chemistry Fundamental and Applied, Faculty of Sciences and Techniques, Moulay Ismaïl University, PB 509, Errachidia, Morocco, email: younesdahmani329@gmail.com*
[d]*Laboratory of Advanced Materials and Process Engineering, Faculty of Sciences, University Ibn Tofail, P.O. Box: 133, Kenitra 14000, Morocco, email: hmmoumossout@gmail.com*

Received 15 July 2023; Accepted 28 October 2023

ABSTRACT

The aim of this work is the study of phenol adsorption in aqueous medium onto raw red clay (RRC) and treated red clay (TRC) from the Drâa–Tafilalet region. The treated clay was obtained by two attacks, the first with hydrogen peroxide and the second with hydrochloric acid. The two samples were characterized by various physico-chemical methods, namely fluorescence-X, Fourier-transform infrared spectroscopy (FTIR), X-ray diffraction (XRD), thermogravimetric analysis, differential thermal analysis, and Brunauer–Emmett–Teller technique. These methods indicate that the clay is mainly composed of silica, and alumina, for which chemical treatment is justified by the elimination of carbonate and the increase in a special surface area from 40.962 for RRC to 64.264 for TRC. Phenol adsorption tests showed that equilibrium was reached after 200 min of agitation for adsorbents at different temperatures (30°C, 40°C, and 50°C), with maximum adsorption yields equal to 3.53 for RRC and 4.88 for TRC. The non-linear modeling indicates that the pseudo-second-order model describes the adsorption kinetics. In contrast, the corresponding adsorption isotherms follow the Langmuir and Redlich–Peterson models for the two adsorbents. This shows that the adsorption is done initially on the monolayer and then moved on to the multilayer. FTIR and XRD analysis of the adsorbents after adsorption show that the phenol was adsorbed and penetrated into the interlayer space, resulting in an expansion of the interlayer space.

Keywords: Adsorption; Phenol; Isotherm; Kinetic; Mechanism; Non-linear model

1. Introduction

The problem of water and soil pollution was not as serious in the past as it is now. Due to the development of industry, this problem began with the Industrial Revolution. Water resources are scarce, and the amount of water used for domestic and industrial purposes is increasing. The discharge of domestic garbage and untreated industrial wastewater into water bodies is the main source of water pollution. Therefore, the treatment and reuse of

* Corresponding author.

wastewater are the ultimate solutions to this problem. The State Environmental Protection Administration of China has classified organic compounds in water [1]. Phenol has low solubility, low ionization capacity, and low vaporization pressure [1]. In general, phenols are considered priority pollutants because they are harmful to organisms at low concentrations and many have been classified as dangerous pollutants due to their harmful effects on human health. The United States Environmental Protection Agency (EPA) requires a reduction of the phenol content in wastewater to less than 1 mg/L [2].

The different water treatment technologies used to remove phenolic pollutants are destructive processes such as destructive oxidation with ozone [3], hydrogen peroxide [4], or manganese oxides [5], and recovery processes such as adsorption by porous solids [6], membrane separation [7] and solvent extraction [8]. For the treatment of the aqueous phase by adsorption, activated carbon is the most widely used adsorbent. However, it is very expensive and has high operating costs [7]. Therefore, in recent years, considerable attention has been paid to the study of different types of low-cost materials in order to remove pollutants from the water phase. Many researchers have studied the adsorption of phenol on clays. Indeed, according to the chemical composition and the crystalline structure, clays can be classified into several families, the most important of which are the kaolinite family, the illite family, and the smectite family, which have the highest adsorption capacity [9–11].

In contrast, the physical and chemical properties of natural clays, such as cation exchange capacity, specific surface area, porosity and surface acidity, are closely related to their atomic structure, intercrystallite texture and chemical composition. These properties are often modified in order to obtain a very specific adaptation to a well-defined use. Substitution of exchangeable cations (cation exchange) [12–14], insertion of organic molecules [15] and treatment by the acid attack are increasingly practiced on clay materials [16–21]. Clays activated by the acid attack are generally used for the preparation of bleaching earth [22–25] and acid catalysts [23,26–31]. The effect of the attack by sulfuric acid on the physico-chemical characteristics of clays is very dependent on the treatment conditions (concentration of the acid, temperature, contact time, etc.). The use of the concentrated acidic solution at relatively high temperatures for long periods generally leads to deep destruction of the crystal lattice of the clay with the formation of a significant amount of amorphous silica. The attack of the clay by the acid takes place according to a well-defined mechanism, which begins with the adsorption of sulfuric acid on the surface of the solid to lead to the substitution of the exchangeable ions by the protons. The exchanged protons then diffuse towards the active sites of the treated solid where the chemical reactions take place (cutting of existing chemical bonds and formation of other bonds). The soluble products of these chemical reactions are subsequently desorbed in the liquid phase [32,33]. The chemical attack is accompanied by the gradual dissolution of the solid, which can then lead to dislocation, or even the collapse, under severe attack conditions, of the crystal lattice and the formation of amorphous silica [34,35]. The structural cations of the clay (Al^{3+}, Mg^{2+}, Fe^{2+}) are replaced, during the acid attack, by H^+ protons to lead to a substantial increase in the surface acidity of the clay.

The aim of this study is the valorization of raw red clay (RRC) and treated red clay (TRC), by the chemical process using H_2O_2 and HCl, in the retention of phenol in aqueous solution using adsorption experiments, red clay has proven to be particularly efficient at removing phenol from wastewater [36,37]. Before their use, the adsorbents were characterized by X-ray fluorescence, Fourier-transform infrared spectroscopy (FTIR), X-ray diffraction (XRD), thermogravimetric analysis/differential thermal analysis (TGA/DTA) and Brunauer–Emmett–Teller (BET). In order to better divine the experimental kinetic and isothermal data for the adsorption of phenol onto RRC and TRC, the linear and non-linear forms of the different kinetic and isothermal models were used. The R^2 (coefficient of determination), the Δq (%) (standard deviation) and the χ^2 (chi-square) of the tests were calculated to determine the validity of the different forms of these models. The mechanism investigation was discussed by studying the adsorption isotherms, as well as the analysis of the adsorbents before and after the adsorption of phenol by FTIR and XRD.

2. Materials and methods

2.1. Raw and treated clay

The clay used for this work was taken from the Atlas of Morocco (Goulmima). The clay is crushed and sieved using a sieve with known openings. Only particles smaller than 315 μm are retained. The chemical treatment of raw clay has undergone two physical and chemical steps: the first physical step is to disperse 50 g of raw clay in 3 L of deionized water and stir the mixture at room temperature for 3 h (20°C–22°C). At this stage, the particles no longer flocculate but are in the form of a suspension. The suspension is allowed to stand for 6 h for precipitation. After standing for 6 h, carefully, we sucked out the suspension of 15 cm above the sediment. This operation is repeated two more times. The second (chemical) step proceeds: After the clay is recovered, it is dispersed in 30 mL of hydrogen peroxide H_2O_2, and then heated to 70°C for 30 min, and then hydrogen peroxide (H_2O_2) removes organic matter. At a temperature of 25°C, the ratio of 10 g clay/100 mL solution of hydrochloric acid (5 mol/L) was treated for 3 h. The clay/acid mixture is separated by centrifugation. The solid phase was washed twice with hot distilled water to remove excess acid impregnated on its outer surface, dried in an oven at 80°C for 48 h, crushed, and then stored away from moisture until the moment of use.

2.2. Characterizations of samples

X-ray fluorescence was performed using an "Axion" type X-ray fluorescence spectrometer with a 1 kW wavelength dispersion. This chemical analysis was performed at the UATRS Laboratory, CNRST in Rabat. XRD patterns were reported using an X'PERT MPD PRO wide-angle X-ray powder diffractometer provided with a diffracted beam monochromator, and Ni filtered CuKα radiation (λ = 1.5406 Å). The 2θ angle was scanned between 4° and 30° range with a counting time of 2.0 s at steps of 0.02°. RRC and TRC were characterized by using a Fourier-transform infrared

spectrometer (VERTEX 70). Samples were prepared in KBr slices in the usual way from very well-dried mixtures of approx. 4% (w/w). The FTIR spectra were recorded from 4,000 to 400 cm^{-1} and the thermogravimetric analysis/differential thermal analysis analyses were performed under air atmosphere in a simultaneous LABSYS evo TGA/DTA thermal analyzer. The samples were heated linearly ($T = T_0 + \beta \cdot t$) from room temperature to 900°C at the heating rate 20°C/min. Nitrogen adsorption measurements were obtained using a Micromeritics ASAP 2010 (Bruker Co., Germany) to obtain the textural parameters. The cation exchange capacity (CEC) was determined by using the cobaltihexamine chloride method [38], which is based on the measurement of the Co remaining in the solution after the exchange of $[C_0(NH_3)_6]^{3+}$ ions.

2.3. Batch adsorption experiments

0.2 g of each type of adsorbent is introduced into a 50 mL bottle containing 20 mL of phenol. The initial phenol concentrations are between 10 and 50 mg/L for the raw red clay (RRC) and treated red clay (TRC) adsorbents. The kinetic study was carried out without pH adjustment. The suspensions were stirred using a rotary stirrer at 250 rpm. The samples are taken at a well-defined time interval. The supernatant obtained after centrifugation was filtered and then analyzed using a visible UV spectrometer at 270 nm. The residual concentration of C_e is determined from the UV/visible spectrometer calibration curve. Eq. (1) is used to determine the amount adsorbed:

$$Q_{\text{ads}} = \frac{C_0 - C_e}{m_{\text{adsorbent}}} \times V_{\text{sol}} \tag{1}$$

where Q_{ads}: adsorption capacity (mg/g), C_0: initial concentration (mg/L), C_e: residual concentration (mg/L), m: mass of adsorbent (g) and V_{sol}: volume solution (L).

2.4. Kinetic and isothermal modelling

To determine the phenol adsorption mechanism in both samples, experimental data were mounted using linear and non-linear models, respectively. In fact, the modeling of the adsorption kinetics was carried out by the pseudo-first-order, pseudo-second-order, and Weber and Morris [39,40]. Adsorption isotherms are helpful in understanding the mechanism of adsorption. Although several isotherm equations are available due to their simplicity, in this regard, research has proposed many isotherms that are based on the adsorption system, including Langmuir, Freundlich, and Redlich–Peterson. In this study, the adsorption was performed using non-linear adsorption models by varying the initial concentration to assess the relationship between the amount of phenol adsorbed on the adsorbents and their equilibrium concentration in aqueous solution. The equations of these three modules [41]:

Pseudo-first-order: $\ln(q_e - q_t) = \ln(q_e) - k_1 t \; ; \; q_t = q_e\left(1 - e^{-k_1 t}\right)$ (2)

Pseudo-second-order: $\frac{t}{q_t} = \frac{1}{q_e^2 k_2} + \frac{1}{q_e} t \;\; ; \;\; q_t = \frac{q_e^2 k_2 t}{q_e k_2 t + 1}$ (3)

Weber and Morris: $q_t = k_{\text{id}}\sqrt{t} + C_i$ (4)

Langmuir: $\frac{C_e}{q_e} = \frac{1}{K_L q_m} + \frac{C_e}{q_m} \;\; ; \;\; q_e = \frac{q_m K_L C_e}{1 + K_L C_e}$ (5)

Freundlich: $\ln(q_e) = \ln(K_F) + \frac{1}{n}\ln(C_e) \;\; ; \; q_e = K_F C_e^{1/n}$ (6)

Redlich – Peterson: $\frac{C_e}{q_e} = \frac{1}{A} + \frac{C_e^{\beta}}{q_m}$;

$q_e = \frac{AC_e}{1 + K(C_e)^{\beta}}$ with $A = K_R q_m$ (7)

Where q_m: adsorption capacity at equilibrium (mg/g); C_e (mg/L): residual concentration at equilibrium and K_L·(L/mg) represent the ratio between the adsorption and desorption rate constant. k_d and C are the intraparticle diffusion rate constant and the layer thickness, respectively. K_F and n are Freundlich's constants that express the adsorption capacity and the intensity, respectively. K and β (0 < β < 1) are the R-P constants.

The calculation of error confirmed the efficacy of these model analyses, such as the determination factor (R^2), standard deviation [Δq (%)] and the quantification analysis (χ^2) [41]:

$$\Delta q(\%) = 100 \times \left\{ \frac{\sum_{i=1}^{n}\left[\left(q_{\text{exp}} - q_{\text{cal}}\right)/q_{\text{exp}}\right]^2}{n-1} \right\}^{1/2} \tag{8}$$

$$\chi^2 = \sum_{i=1}^{n} \frac{\left(q_{\text{exp}} - q_{\text{cal}}\right)^2}{q_{\text{cal}}} \tag{9}$$

$$R^2 = \frac{\sum_{i=1}^{n}\left(q_{\text{cal}} - \overline{q_{\text{exp}}}\right)^2}{\sum_{i=1}^{n}\left(q_{\text{cal}} - \overline{q_{\text{exp}}}\right)^2 + \sum_{i=1}^{n}\left(q_{\text{cal}} - \overline{q_{\text{exp}}}\right)^2} \tag{10}$$

3. Results and discussion

3.1. Characterization of adsorbent

3.1.1. X-ray fluorescence

The chemical composition is given as a percentage of the oxides' mass. The results obtained for RRC and TRC, presented in Table 1, show that SiO_2 and Al_2O_3 are the main constituents of the two samples. The SiO_2 content (72.42% after treatment with HCl) increases, and the content of AlO_2, MgO and Fe_2O_3 decrease. The decrease in the content of Fe_2O_3 and MgO is significant. The Na_2O and K_2O content in the solids remain almost constant during processing. The presence of these elements in the sample, and a significant amount of Al is due to the persistence of silicate alumina phases such as illite, kaolinite and impurities such as feldspars, which are insoluble in acid solutions [42]. The elimination of carbonates

Table 1
Chemical composition of raw red clay and treated red clay

Oxide/Mass (%)	SiO_2	Al_2O_3	CaO	MgO	Fe_2O_3	K_2O	Na_2O	TiO_2	L.O.I.
Raw red clay	52.9	15	4.67	4.31	7.16	5.59	0.283	0.652	8.78
Treated red clay	72.42	7.41	0.05	2.05	4.12	5.75	0.280	0.30	7.62

L.O.I.: Loss on ignition

and organic matter by chemical treatment is justified by the reduction of the loss of ignition from 8.78% to 7.62% and the calcium oxide content from 4.67% to 0.05%.

3.1.2. Fourier-transform infrared spectroscopy

The infrared spectra recorded for RRC and TRC presented in Fig. 1 show the absorption bands of hydroxyl groups (OH), the Si–O bond and M–OH (with M = Al, Mg, Fe). The comparison of the spectra obtained with those in the literature reveals similarities, which easily allowed us to assign the frequencies of vibration observed. The bands at 3,420 and 1,640 cm^{-1} correspond, to the valency and deformation vibration of water used in the hydration of clay [43]. Deformation bands appear around 520 cm^{-1} for Si–O–Al vibration and 465 cm^{-1} for Si–O–Si [44,45]. The infrared spectrums contain additional bands at 780 cm^{-1}, revealing the presence of the quartz [43], and a band at 1,420 cm^{-1} corresponding to the carbonate. In addition, we note the presence of an intense broadband centered at 1,020 cm^{-1} that can be assigned to the Si–O vibration of the tetrahedral sheet. The comparison of FTIR spectra of RRC and TRC indicates the disappearance of certain absorption bands of the RRC spectrum, mainly the band located at 1,420 cm^{-1}, following the disappearance of impurities; these results confirm that of the chemical analysis.

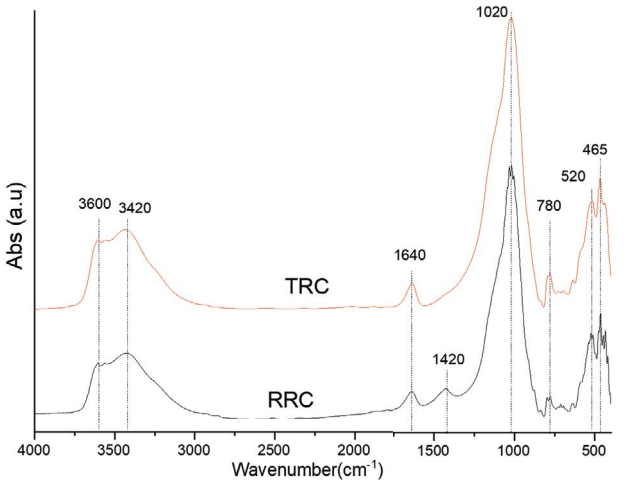

Fig. 1. Fourier-transform infrared spectra of raw red clay and treated red clay.

3.1.3. X-ray diffraction

The constituent phases of clay minerals, as well as the structural changes resulting from acid treatment, were evaluated by XRD analysis. The results are shown in Fig. 2. Indeed, the diffractogram of RRC indicates that the latter is mainly composed of illite, kaolinite quartz, calcite, dolomite, and feldspar. The chemical treatment process causes the degradation of calcite and dolomite [46]. However, it improves the peak of illite. Basal quartz thoughts persist, but their intensity decreases significantly. After treatment, TRC is relatively depleted in organic matter and carbonate. From the TRC spectrum, we also notice that the acid concentration used did not destroy the crystal structure of the clay.

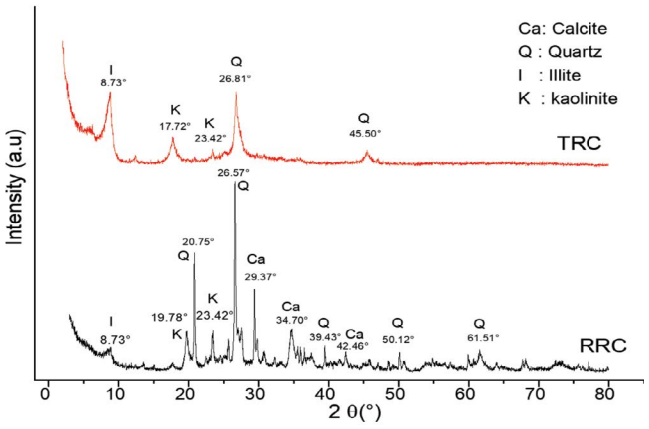

Fig. 2. X-ray diffraction spectra of raw red clay and treated red clay.

3.1.4. Thermogravimetric analysis/differential thermal analysis

The thermal analysis of RRC and TRC confirms the results obtained by other analysis techniques, particularly XRD and FTIR. The thermogravimetric analysis curves (Fig. 3) make it possible to follow the loss of adsorbent mass. Three mass losses are observed for RRC and only two for TRC. Moisture water loss occurs at 75°C and 98°C, inter-leaf water loss occurs at 167°C and 274°C. RRC decarbonisation occurs at 775°C. This loss does not appear for the TRC sample; it can be explained by the removal of carbonates by the acid treatment. In addition, endothermic peaks around 559°C–575°C were due to the transformation of α quartz into β quartz [47].

3.1.5. Brunauer–Emmett–Teller

The specific surface area and pore size distribution of adsorbents are among the most important parameters describing the quality of adsorbents because they directly

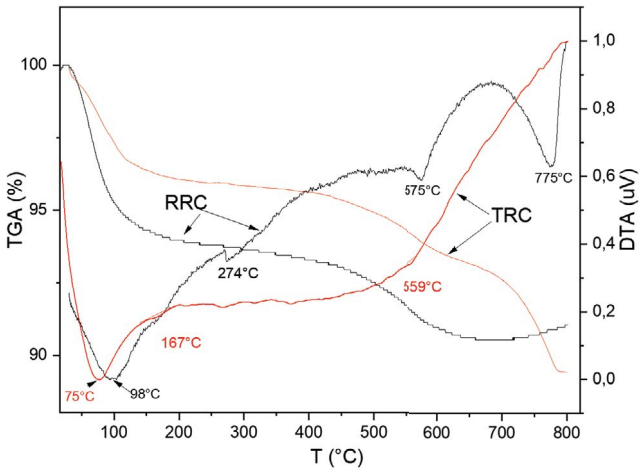

Fig. 3. Thermogravimetric analysis/differential thermal analysis of raw red clay and treated red clay.

Table 2
Textural characteristics of raw red clay and treated red clay

	Brunauer–Emmett–Teller		
	Specific surface area (m^2/g)	Volume (cm^3/g)	Diameter (Å)
Raw red clay	40.962	0.1217	136.15
Treated red clay	64.264	0.0402	31.90

affect their ability to retain analytes. The BET area, the pore size, and the total pore volume obtained from the analyses (Table 2) were 40 m^2/g, 136.15 Å, 0.1217 cm^3/g and 64 m^2/g, 31.90 Å, 0.0402 cm^3/g, respectively for RRC and TRC. The isotherms obtained in Fig. 4 are type IV. According to the International Union of Pure and Applied Chemistry classification, it is accepted that they are characteristics of mesoporous solids. H_3-type hysteresis characterizes porous solids whose pore size, distribution, and shape are not uniform. The increase in the BET surface area of TRC indicates that the porous texture has changed. Usually, this increase results from the action of the acid, which causes the impurities to dissolve and the replacement of the exchangeable cations by protons. This phenomenon causes the departure of the elements Al^{3+}, Mg^{2+} and Fe^{3+} from octahedral or tetrahedral sites. Thus, the empty spaces occupied by these metals give rise to micropores.

3.1.6. Cation exchange capacity

The analysis of CEC indicates that RRC has a lower CEC (16.64 meq/100 g) than TRC (21.74 meq/100 g). Indeed, the chemical treatment of RRC using the HCl solution was accompanied by a substantial gradual increase in the amount of SiO_2 and a decrease in that of Al_2O_3. The increase in CEC can be interpreted as resulting from the disaggregation of clay platelets by the acid attack. The mineral impurities responsible for the aggregation of platelets would act in two ways: on the degree of division of the grains on the one hand and the spacing of the layers on the other hand. This would limit access to all exchange sites by blocking and inhibiting

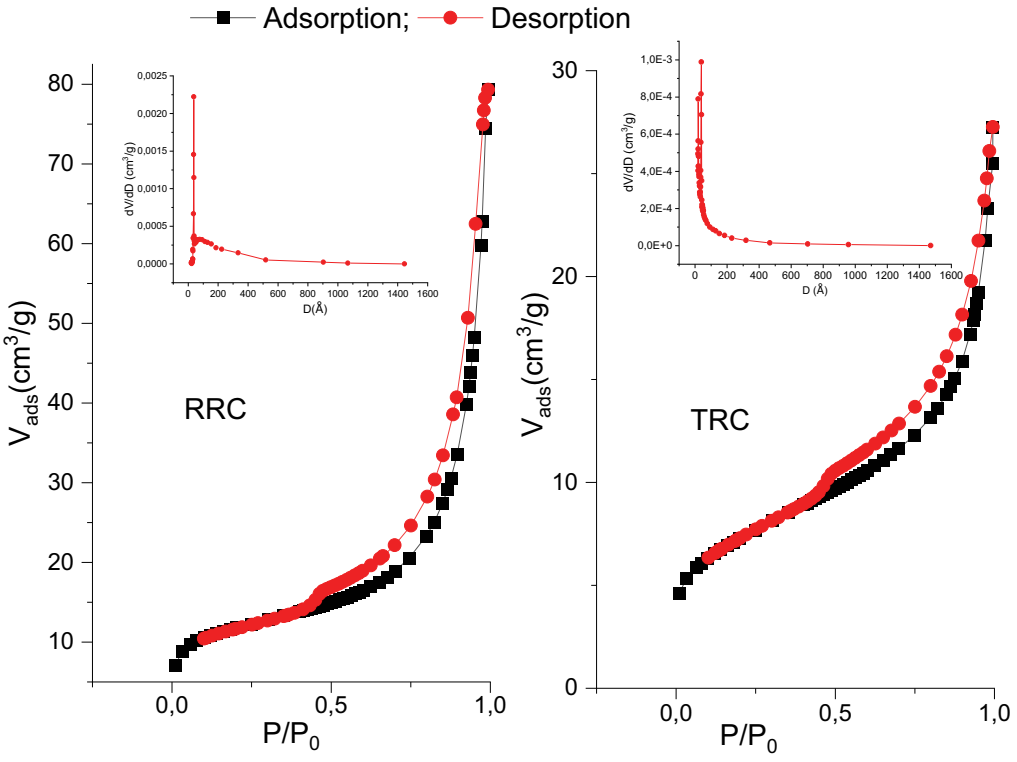

Fig. 4. N_2 adsorption/desorption isotherms of raw red clay and treated red clay.

the phenomenon of bloating. In the first heating stage, the moderately active acids could dissolve these impurities and allow the leaflets to spread apart, thus accessing more exchange sites. The same phenomenon occurs during activation by strong acids. In this case, the increase in the CEC value is brief because of the rapidity of the attack kinetics of the mineral impurities contained in the clay. In conclusion, we can promote access to an additional number of exchange sites, increasing the apparent value of the CEC.

3.1.7. pH_{pzc}

Fig. 5 shows that the pH_{pzc} of RRC and TRC equals 7.8 and 4.94, respectively. The overall surface charge is positive for solutions with a pH lower than these values and negative for solutions with a pH higher than pH_{pzc}. To interpret our results, we compare them with the mechanisms proposed by Yariv et al. [48,49] to explain the fixation of phenol on the surface of clays. At pH greater than pH_{pzc} and above pKa (= 9.89), the dissolution of phenol in water releases ions of a negative charge (phenolate ions). In this case, phenol is an ionic compound, so electrostatic repulsive interactions take place between the phenolate ions and the adsorption sites (Fig. 6). In the second type of interaction, since the adsorbate and the adsorbent have the same sign of charge, compensating ions of opposite charges present in the clay or solution can form bridges between the adsorbate and the adsorbent.

On the contrary, at a pH below pH_{pzc}, the phenol and silanol groups on the surface of the adsorbent were in protonated form, allowing the adsorption of the phenol molecules to the surface silanol groups by the hydrogen bond. On the other hand, aluminol has an amphoteric character; in an acidic environment, it plays the role of a base. Therefore, it can be attracted by electrostatic attraction (Fig. 7). A second involves a hydrogen bond between the water hydration molecules of the interfoliar cations and the functional group of phenol.

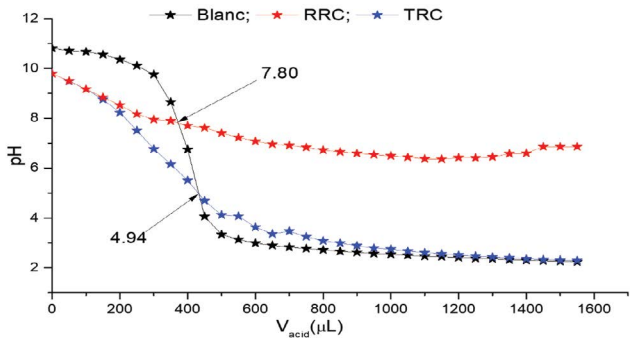

Fig. 5. pH_{pzc} of raw red clay and treated red clay.

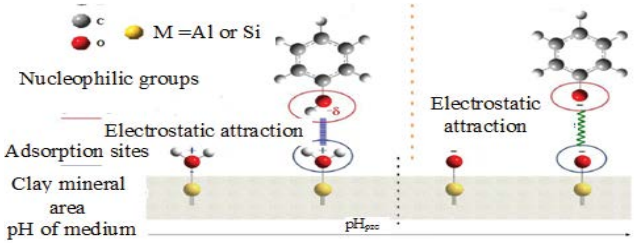

Fig. 6. Illustration of the adsorption mechanism of phenol by electrostatic forces.

3.2. Adsorption study

3.2.1. Adsorption kinetic

In order to see if equilibrium was reached, the phenol adsorption onto RRC and TRC was studied vs. the contact time at different temperatures (30°C, 40°C and 50°C) (Fig. 8). The results indicate that the amount of phenol adsorbed by RRC and TRC increases during the first-time interval for the three temperatures studied. However, this increase was marked early in the reaction, after the extent of adsorption gradually decreased. Initially, many active sites were available on the adsorbent surface; and a significant increase in adsorption occurred, but these sites became occupied over time, making adsorption slow [50]. Equilibrium was reached for the adsorption of phenol on the two samples (RRC and TRC) after 200 min of contact for all temperatures. The phenol may have adsorbed to the surface. These results also indicate that the amount of phenol adsorbed on TRC is high, which shows the value of treating the clay with acid. This increase can be explained by the positive charge of the TRC surface at pH = 4, which comes into contact with the nucleophilic groups through electrostatic interactions and hydrogen bonds. The amount of phenol adsorbed on both adsorbents increases with increasing temperature, indicating that the process is apparently endothermic. This can be explained based on hydrogen bonding. In aqueous solutions of phenol, there is a strong hydrogen bond between the phenol molecule and water, resulting in appreciable solubility. These hydrogen bonds break at higher temperatures, making the phenol less soluble and, therefore, exhibit a higher tendency to attach to the surface of the adsorbent instead of remaining in solution [51]. Similar results have been found in other studies [52]. The increase in adsorption capacity suggests that the active surface centers available for adsorption increased with increasing temperature [53].

The modeling of the phenol adsorption kinetics on the two solids was performed by linear (not shown) and non-linear (Fig. 8) pseudo-first-order and pseudo-second-order models. Table 3 gathers the parameters of the two forms (linear and non-linear) of these two models. Indeed, a weak correlation was obtained for the linear and non-linear form of the pseudo-first-order model for the two solids. Therefore, indicate that the adsorption of phenol on

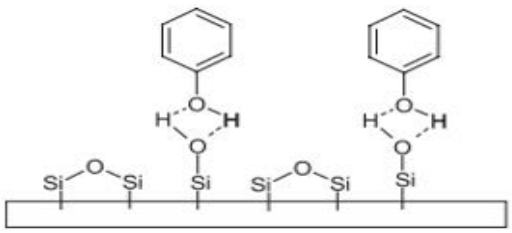

Fig. 7. Illustration of the adsorption mechanism of phenol by hydrogen bonds.

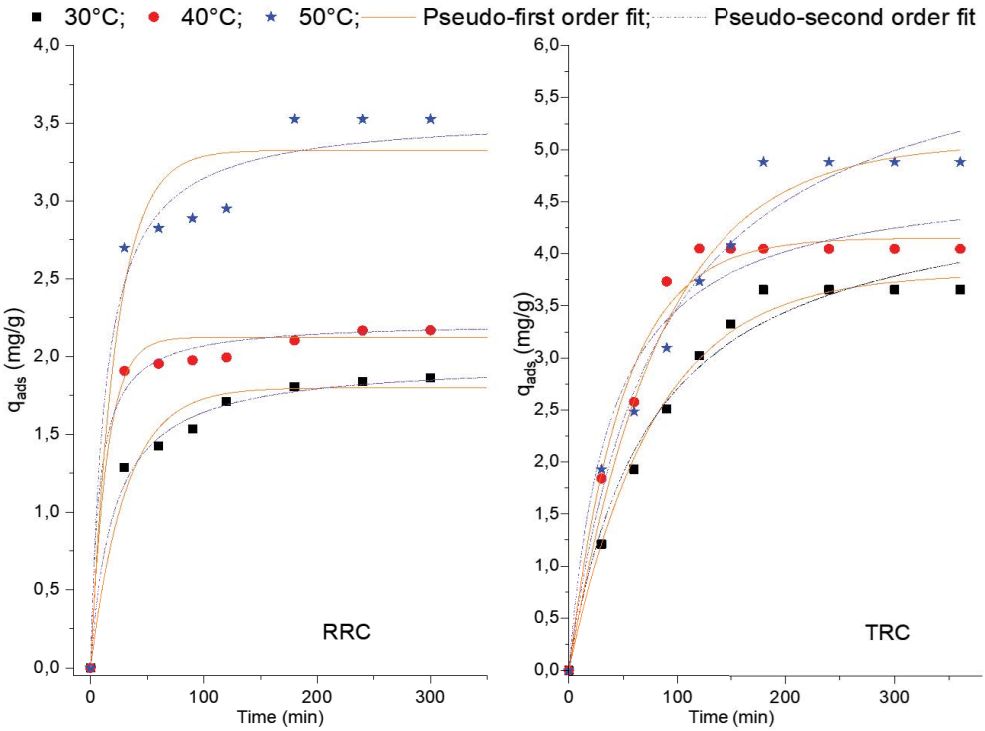

Fig. 8. Kinetic study of phenol adsorption with non-linear models of pseudo-first-order and pseudo-second-order onto raw red clay and treated red clay.

Table 3
Kinetic parameters of linear and non-linear modelling of phenol adsorption at different temperatures onto raw red clay and treated red clay

Sample		Raw red clay						Treated red clay					
Models		Linear equations			Non-linear equations			Linear equations			Non-linear equations		
	q_{exp} (mg/g)	1.88	2.44	3.53	1.88	2.44	3.53	3.66	4.05	4.88	3.66	4.05	4.88
	T (°C)	30	40	50	30	40	50	30	40	50	30	40	50
PFOM	q_e (mg/g)	1.59	1.94	2.22	1.80	2.13	3.33	5.07	0.989	6.33	3.814	4.157	5.066
	K_1 (min^{-1})	0.017	0.014	0.022	0.032	0.070	0.045	0.026	0.026	0.022	0.013	0.020	0.012
	Δq (%)	36.76	92.91	120.15	7.596	6.83	9.438	218	189	292	3.67	6.05	8.80
	χ^2	–4.278	–3.210	–2.939	0.059	0.076	0.179	–3.30	–204	–10.10	0.032	0.086	0.179
	R_1^2	0.914	0.540	0.805	0.970	0.960	0.943	0.801	0.609	0.790	0.993	0.983	0.981
PSOM	q_e (mg/g)	2.00	2.42	3.75	1.98	2.22	3.56	4.54	4.48	6.07	4.733	4.796	6.368
	K_2 (g/mg·min)	0.023	0.022	0.013	0.027	0.06	0.021	0.003	0.008	0.002	0.003	0.005	0.002
	Δq (%)	4.55	11.843	8.553	3.836	5.329	6.424	7.71	11.13	7.29	7.11	9.47	7.179
	χ^2	0.442	2.347	0.903	0.015	0.046	0.083	1.86	2.49	1.289	0.097	0.210	0.143
	R_2^2	0.999	0.988	0.996	0.993	0.976	0.975	0.980	0.987	0.981	0.980	0.960	0.978

the two adsorbents does not follow the kinetics of pseudo-first-order. The linear and non-linear forms of pseudo-second-order kinetic models were applied to the experimental data. The correlation coefficient (R^2) values of RRC and TRC, found are close to 1, indicating the best fit of this model on the phenol adsorption data. The theoretical results obtained for the quantity of phenol adsorbed at equilibrium are better suited to the experimental data for pseudo-second-order kinetics that can be explained by the low values of Δq. For the adsorption of phenol to the two adsorbents, the pseudo-second-order model can describe the adsorption method quite appropriately compared to the pseudo-first-order model.

3.3. Intraparticle diffusion

The results of the intraparticle diffusion model are shown in Fig. 9, and in Table 4, the plots of the lines do

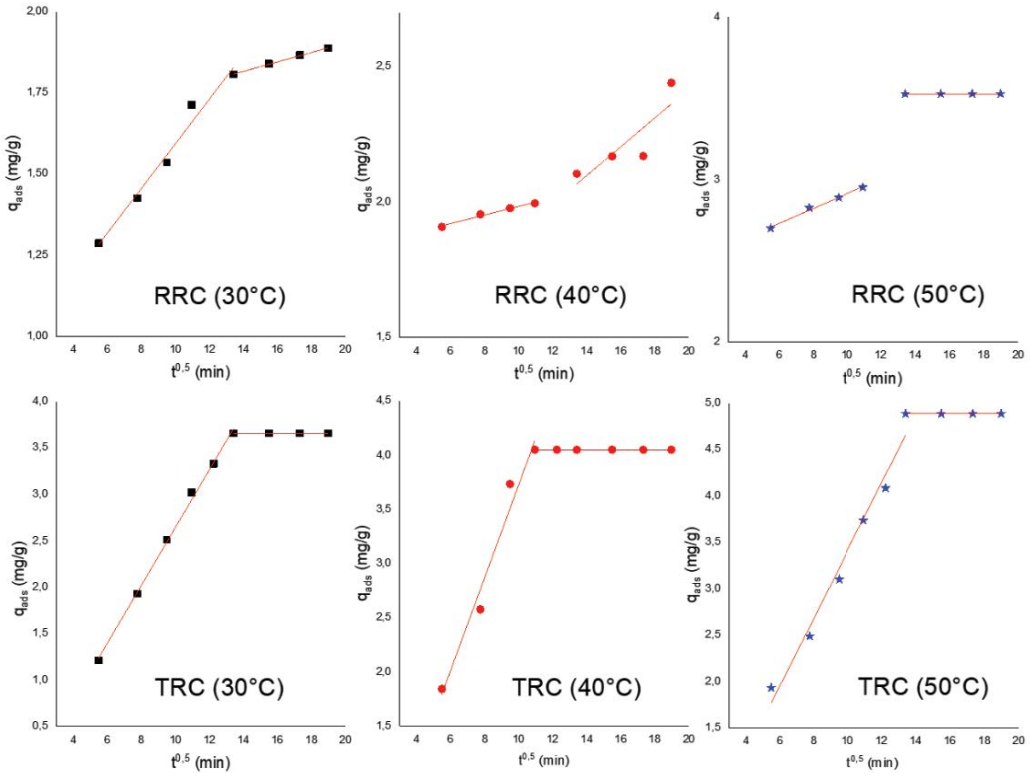

Fig. 9. Intraparticle diffusion model for phenol adsorption onto raw red clay and treated red clay.

Table 4
Parameters of the intraparticle diffusion model equations

Sample		Step 1				Step 2			
	T (°C)	k_{d1} (mg/g·min)	C_1	R_1^2	SD	k_{d2} (mg/g·min)	C_2	R_2^2	SD
Raw red clay	30	0.069	0.91	0.977	0.004	0.015	1.61	0.998	6.22e-6
	40	0.0158	1.825	0.981	8.026e-5	0.053	1.353	0.725	0.018
	50	0.045	2.46	0.991	3.12e-4	0	3.53	1	0
Treated red clay	30	0.311	–0.470	0.998	0.010	0	3.658	1	0
	40	0.428	–0.553	0.969	0.095	0	4.049	1	0
	50	0.363	–0.226	0.978	0.129	0	4.881	1	0

not go through the origin, which means that the adsorption involved the intraparticle diffusion does not constitute the step limiting adsorption. Other kinetic models can control the rate of adsorption [54].

Observation of the figures shows that the adsorption takes place in two stages: adsorption on the surface of the materials and then intraparticle diffusion. The first step, being faster than the second, is attributed to the adsorption on the external surface; it corresponds to the diffusion in the boundary layer of the solute molecules, the adsorbate migrating from the solution to the external surface of the adsorbent. The second part is attributed to intraparticle diffusion, which determines the speed of control of the adsorption mechanism. Intraparticle diffusion slows down, leading to maximum adsorption and a very low concentration of adsorbate in solution. The values of intercept C (Table 4) give an idea of the thickness of the boundary layer, the larger interception, the greater boundary layer effect.

3.4. Equilibrium isotherm

Fig. 10 represents the plot of q_{ads} vs. C_e at different temperature values (30°C, 40°C and 50°C) using the experimental value and predicted by non-linear models. Table 5 shows the values of the parameters of a non-linear Langmuir, Freundlich and Redlich–Peterson model.

3.4.1. Langmuir isotherm

The R^2 values of RRC and of TRC were considered satisfactory, showing the suitability of the model on the adsorption experiment. The dimension less constant R_L is

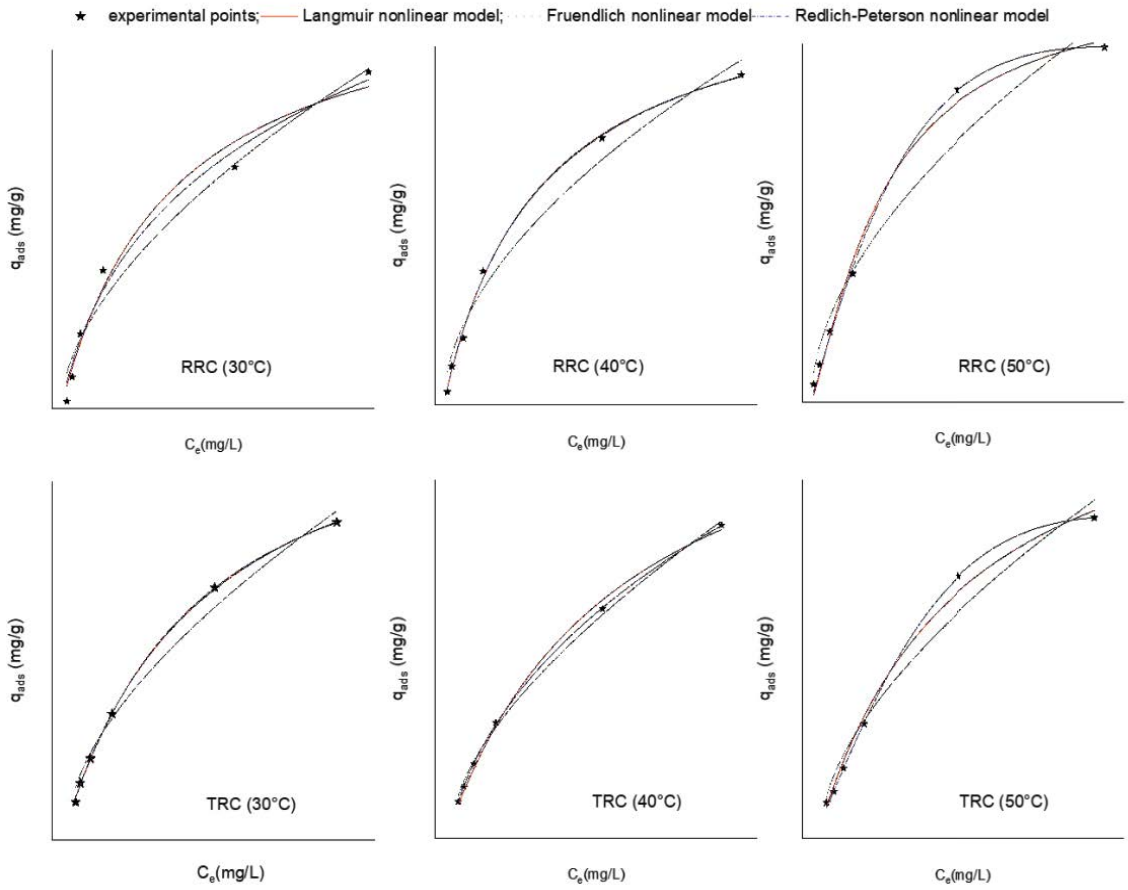

Fig. 10. Phenol adsorption isotherm onto raw red clay and treated red clay at different temperature with, non-linear fit of Langmuir, Freundlich and Redlich–Peterson models.

Table 5
Model parameters for the phenol adsorption onto raw red clay and treated red clay at different temperatures

Model	Sample	Raw red clay			Treated red clay		
	T (°C)	30	40	50	30	40	50
Langmuir	q_m (mg/g)	28.152	30.232	34.844	37.650	46.791	49.971
	K_L (L/mg)	0.008	0.009	0.008	0.005	0.004	0.006
	R^2	0.981	0.998	0.994	0.999	0.998	0.994
	χ^2	1.291	0.172	0.412	0.166	0.228	0.580
	R_L	0.999	0.999	0.999	0.999	0.999	0.999
	Δq (%)	103.41	14.92	14.846	27.468	12.895	19.569
Freundlich	K_F (mg/g)	0.720	1.002	1.071	0.623	0.639	0.864
	$1/n$	0.581	0.541	0.549	0.631	0.654	0.632
	R^2	0.974	0.980	0.961	0.987	0.998	0.972
	χ^2	2.511	1.527	1.765	1.206	0.358	1.893
	Δq (%)	185.363	69.042	38.765	81.198	25.572	38.728
Redlich–Peterson	K_{P-R}	0.041	0.010	2.678e-4	0.004	0.072	5.594e-5
	A	0.284	0.269	0.209	0.186	0.312	0.214
	β	0.762	0.980	1.518	1.056	0.622	1.730
	R^2	0.984	0.998	0.998	0.999	0.999	0.999
	χ^2	1.508	0.177	0.611	0.154	0.011	0.861
	Δq (%)	126.76	15.624	22.121	25.610	2.482	24.321

calculated using Langmuir's constant, and the initial concentration represents the fit of the model for a particular system. If the value of R_L is between 0 and 1, the system is considered suitable for adsorption purposes. The results reported in Table 5 show that the value of R_L for all temperatures is within this range. Furthermore, the experimental data and the predicted results obtained for the present work were found to correlate closely with low values of the residual sum of the square such as for RRC ($\chi^2 \leq 0.580$) and for TRC ($\chi^2 \leq 1.291$), this which makes this model applicable to the present work.

3.4.2. Freundlich isotherm

The parameters calculated for the Freundlich isotherm using its non-linear form are given in Table 5. In the present adsorption study, the values of $1/n$, for the non-linear approach are less than 1, which indicates that phenol was adsorbed favourably by RRC and TRC for all temperatures studied [54]. Likewise, the values of R^2 obtained are significant.

3.4.3. Redlich–Peterson

Due to the higher R^2 values listed in Table 5, the Redlich–Peterson model gave the best fit at temperatures 30°C, 40°C and 50°C for RRC ($R^2 > 0.98$) and for TRC ($R^2 > 0.98$). The values of the β exponent obtained for the adsorption process on RRC and TRC are 0.622 at 40°C and 0.762 at 30°C, respectively. Indeed, theoretically, the Redlich–Peterson model is based on the theories of Langmuir and Freundlich. This correlation with the experimental results for the adsorption of phenol on the two solids indicates that the adsorption is initially on the monolayer and then passes to the multilayer.

3.4.4. Error analysis for equilibrium isotherms

In order to verify the fit of the adsorption model to the experimental data, error functions are used [55]. In the present work, two error functions were applied to the non-linear data forms by minimizing the error function in a concentration range. The comparison of the error functions shows that the non-linear form of the Freundlich isotherm was not considered suitable for the adsorption of phenol by RRC and TRC due to the significant values of the error functions. However, the Langmuir and Redlich–Peterson isotherms were able to perfectly describe the experimental data with low values for the error functions.

$$\chi^2(\text{Freundlich}) > \chi^2(\text{Langmuir}) > \chi^2(\text{Redlich}-\text{Peterson})$$
$$\Delta q(\text{Freundlich}) > \Delta q(\text{Langmuir}) > \Delta q(\text{Redlich}-\text{Peterson})$$

3.5. Thermodynamics studies

the adsorption activation energy representing the minimum energy the reactants must have for the reaction to proceed was determined by the Arrhenius relationship. Indeed, the variation of the pseudo-second-order rate constant as a function of temperature is expressed by the following relation:

$$\ln(K_2) = \ln(A) - \frac{E_a}{RT} \tag{11}$$

where E_a is the Arrhenius activation energy of adsorption; A the Arrhenius factor; R is the gas constant and is equal to 8.314 J/mol·K, and T is the temperature in K. When $\ln K_2$ is plotted vs. $1/T$ (the curves are not shown), we obtain a line with a slope $-E_a/R$. The magnitude of the activation energy results in a type of adsorption, which is primarily physical or chemical. The range of 5–40 kJ/mol of activating energies indicates a mechanism of physisorption while a range of 40–800 kJ/mol suggests a mechanism of chemisorption [56]. The result obtained in this study indicates that E_a (RRC) = 28.14 kJ/mol with R^2 = 0.99 and E_a (TRC) = 38.87 kJ/mol with R^2 = 0.98, which indicates that the nature of the adsorption is physical. values of parameters such as standard enthalpy ($\Delta H°$), standard entropy ($\Delta S°$) and standard free energy ($\Delta G°$) can describe the thermodynamics of adsorption. The standard free energy ($\Delta G°$) is due to solute transfer at the solid–liquid interface. The values of $\Delta H°$ and $\Delta S°$ were calculated using the following equations:

$$\ln(K_L) = -\frac{\Delta H°}{RT} + \frac{\Delta S°}{R} \tag{12}$$

$$\Delta G° = \Delta H° - T\Delta S° \tag{13}$$

By plotting $\ln(K_L)$ vs. $1/T$. The results of the thermodynamic study are presented in Table 6.

The high positive values of the standard enthalpy ($\Delta H°$) as well as the increase in the amount adsorbed with increasing temperature confirm that the adsorption of phenol molecules at the sites of each adsorbent is endothermic in nature, so values of ($\Delta H°$) less than 84 kJ/mol mean that the molecule/particle interactions are physisorption [56]. It is clear that the adsorption entropy of TRC is greater than that of RRC. This means that the adsorption of phenol on the TRC adsorbent results in a less ordered system than the adsorption of phenol on RRC [58]. The negative values of free energy $\Delta G°$ mentioned in the table show that the phenol adsorption process for the two adsorbents is spontaneous and the degree of spontaneity increases with temperature [57].

3.6. Mechanism study

3.6.1. FTIR after adsorption

Fig. 11 shows the FTIR spectra of RRC and TRC before and after the adsorption of phenol. In the FTIR spectra taken before and after the adsorption of phenol, it is clear

Table 6
Thermodynamic parameters for phenol adsorption onto raw red clay and treated red clay

Adsorbents	$\Delta H°$ (kJ/mol)	$\Delta S°$ (J/mol·K)	$\Delta G°$ (kJ/mol)		
			20°C	40°C	60°C
Raw red clay	16.26	67.91	–4.31	–4.99	–5.67
Treated red clay	13.2	55.80	–3.73	–4.29	–4.85

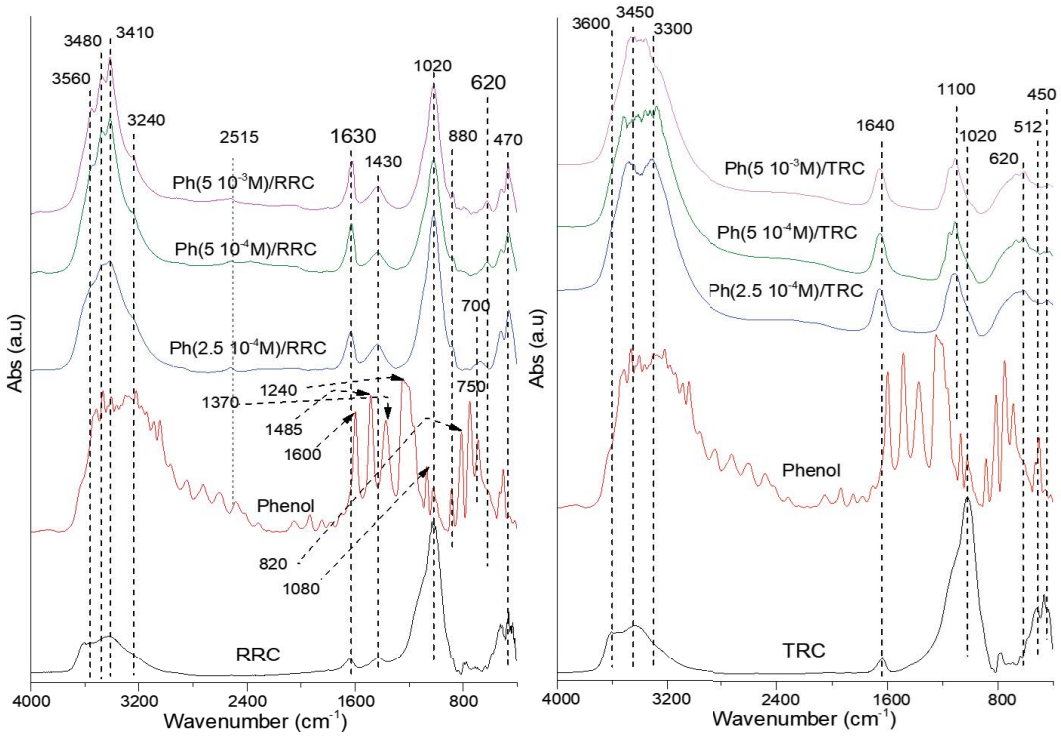

Fig. 11. Fourier-transform infrared spectra before and after phenol adsorption onto raw red clay and treated red clay

that the functional groups characterizing the two adsorbents appeared at approximately the same frequencies for all the different concentrations. There are more peaks in the spectra taken after adsorption of phenol, and these peaks refer to the phenol molecules. Therefore, the increase in absorbance and additional peaks resulting from the phenol molecules which entered the structure of the adsorbent indicate adsorption of phenol from aqueous solution by RRC and TRC. The new peaks observed at 3,240 and 3,300 cm^{-1} on the spectrum of RRC and TRC, respectively correspond to the OH stretching vibrations of the phenol unit [59]. This indicates that the phenol was successfully adsorbed on both materials. Due to the inductive effect of hydrated cations, water molecules can behave like Lewis's acids. This is because phenol forms a hydrogen bond (Fig. 6) with water. Such binding involves a reduction in the energy of the benzene ring delocalization, therefore, the comparison of the ring vibration at 1,600 cm^{-1} of phenol with the same vibration in the spectra after the adsorption of phenol reveals that this band is shifted to a higher frequency 1,630 cm^{-1}. The stretching vibration of C–O which should be 1,240 cm^{-1} cannot be detected either in the case of RRC or in the case of TRC because it overlaps the Si–O adsorption band of the clay. In addition, the OH deformation band reported at 1,370 cm^{-1} in the phenol spectrum, is not detected after adsorption, perhaps due to its overlap with other neighboring band but we observe a band appears at 1,430 cm^{-1}.

3.6.2. X-ray after adsorption

The X-ray analysis diffraction of the powders of the RRC and TRC adsorbents before and after the adsorption of phenol at different concentrations was carried out and presented in Fig. 12. The RRC spectra after adsorption indicate the disappearance of the quartz line which was detected before adsorption at 20.27°, which means in XRD analysis an exfoliation of the interfoliar space of the solid, this is due to the insertion of phenol in this space at a large angle of inclination [60]. Indeed, the average diameter of the phenol molecule is 5 Å, and depending on the mode of its penetration into the interfoliar space, the distance to the quartz plane can only increase if this adsorption mechanism is allowed [61]. For those of TRC after the adsorption of phenol, it is observed that there is a reduction in the spectral intensities without disappearance of the quartz line. This is explained by the fact that the chemical treatment of the clay increased its interfoliar space (BET result) therefore, the concentration of the phenol used was not sufficient to exfoliate the interfoliar space of TRC. It can also be noted that the main peaks, initially detected in the case of the two adsorbents, were detected at the same 2θ angles in the spectra after adsorption with a significant decrease in their intensities. In addition, the new peaks appeared at 2θ = 41.20° and 34.90°, respectively, in the diffractograms of the RRC and TRC adsorbents, indicating that the interactions involved in the adsorption process are not of the same nature. In summary, the combination of FTIR and XRD analyzes provided evidence of the adsorption of phenol on RRC and TRC. This study demonstrated that phenol was adsorbed and penetrated into the interlayer space resulting in expansion of the interlayer space. The same observation can be made from the XRD plots (Fig. 12), which are almost identical at different concentrations, with the reduction of the initial intensities.

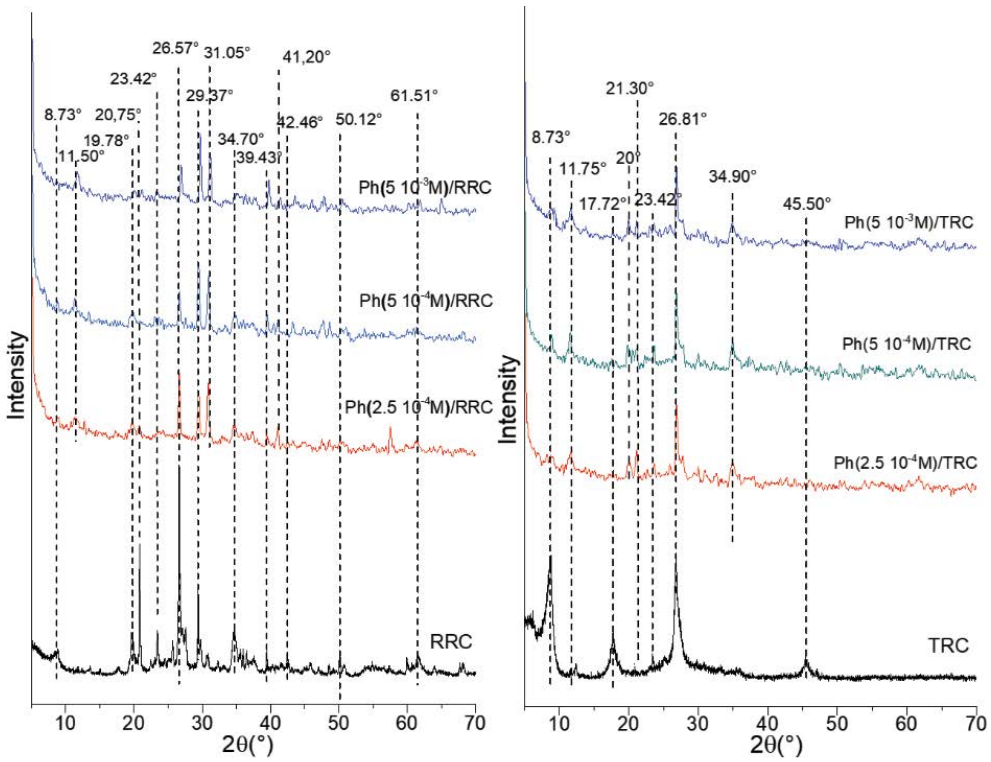

Fig. 12. X-ray diffraction patterns of raw red clay and treated red clay before and after phenol adsorption.

4. Comparative study of our results

Comparison of the results found in the adsorption of phenol by a raw red clay (RRC) and by a chemically TRC with those of previous studies of the adsorption of phenol by a raw yellow clay and calcined yellow clay, shows that the quantity adsorbed by the red clay either in the abutment state or in the treated state is very important for elimination and that the heat treatment slightly improves the capacity of adsorption of a clay unlike chemical treatment.

Table 7 compares the quantities adsorbed by other sources of phenol adsorption in the literature:

5. Regeneration of the adsorbent

Regeneration can be achieved by several methods: Regeneration methods by displacing the pollution, as well as regeneration methods by destroying the pollution.

The most common method of regeneration is thermal regeneration at high temperatures, a pyrolysis process. Pyrolysis technology burns adsorbed organic matter. In our case, given that clays are very abundant and less expensive than other adsorbents, such as activated carbon, regeneration is not necessary.

6. Estimated cost

The most crucial factor when choosing an adsorbent or treatment approach is the expense of the process. Adsorbent cost-effectiveness is the main restriction that must be taken into account when choosing adsorbents in adsorption technologies. The cost of an adsorbent can be influenced by a number of variables, such as the adsorbent's lifetime, local availability, needed processes, treatment conditions, and recyclability or reusability possibilities [65,66].

The total cost of phenol removal was estimated on the basis of the unit price of raw materials, the cost of electricity consumption and the cost of manpower throughout the phenolic solution treatment process (Table 8).

7. Conclusion

The results obtained revealed the treatment effect of clays on the structural and textural properties. Based on measurements of adsorption/desorption isotherms of N_2 at 77 K, it is shown that it is possible to improve the specific surface area without attacking the structure of the clay. The experimental techniques used allowed us to characterize the adsorbents studied and to demonstrate their chemical composition. We have thus established that these adsorbents consist mainly of kaolinite, illite and as associated clay minerals. These results also demonstrated the richness of these adsorbents in quartz, which results in a high proportion of silica. The results showed that RRC and TRC can be used as low-cost adsorbents for the removal of phenol in aqueous media. The adsorption kinetics have been found to follow the pseudo-second-order model and have proposed that intraparticle diffusion is not the critical step in the phenol adsorption mechanism. The adsorption of phenol was found to increase with increasing temperature in the range of 30°C–50°C. The best equilibrium data were described by the Langmuir model at the temperature range of 30°C–40°C for RRC and at the temperature range of 40°C–50°C for TRC and by the Redlich–Peterson model

Table 7
Comparative study of with other published works

Used adsorbent	Temperature (°C)	Adsorbed quantity (mg/g)	References
Raw red clay	40	2.43	Present work
Treated red clay		4.05	
Raw yellow clay	40	1.112	[61]
Calcined yellow clay		1.239	
Activated carbon	–	49.720	[56]
Red mud	30	49.309	[36]
Guava tree bark	50	44.702	[62]
Rice husk	35	50.150	[63]
Rice husk ash	35	13.982	[64]

Table 8
Cost effectiveness study

<table>
<tr><th>Steps</th><th>Cost estimates</th></tr>
<tr><td>I. Cost of raw material
Cost of the raw material is 0.26 MAD/kg corresponding to 0.02522 $/kg</td><td>0.00002522 $/g</td></tr>
<tr><td>II. Cost of crushing the raw material
In our laboratory, we crushed the raw material using a hammer
Cost of manpower:
Cost of manpower = 112.379 MAD/d
Working hours are assumed to be 8 h/d
In 8 h, 100 kg can be crushed
Crushing cost is therefore = 1.124 MAD/kg, corresponding to 0.109 $/kg</td><td>0.000109 $/g</td></tr>
<tr><td>III. Cost of electricity
Electricity tariff = 1.074 MAD/kWh
Electricity consumption – (number of working hours (h) × power (kW) × electricity tariff (MAD/kWh)
Electricity tariff (MAD/kWh)
<table>
<tr><th>Equipment</th><th>Power in W</th><th>Time</th><th>Cost</th></tr>
<tr><td>Mechanical shredder</td><td>1600</td><td>5 min for1 kg</td><td>0.0001432 g</td></tr>
<tr><td>Screening machine</td><td>110</td><td>20 min for 1 kg</td><td>0.03938 g</td></tr>
<tr><td>Agitator</td><td>530</td><td>40 min</td><td>0.37948 operation</td></tr>
<tr><td>Centrifuge</td><td>50</td><td>10 min for 120 mL</td><td>0.0007458 operation</td></tr>
<tr><td colspan="4">Total cost of electricity = 0.41974903 MAD/operation</td></tr>
</table></td><td>0.0407 $/operation</td></tr>
<tr><td>IV. Cost of manpower
Cost of manpower = MAD112.379 M/d
Working hours are assumed to be 8 h/d
In this case, 1 h is needed for an adsorption operation, so 1 h = 0.125 d, and in 1-h the operator can carry out 10 adsorption operations
Cost of manpower = number of hours worked per day × cost of manpower (MAD/d)/number of operations
Manpower cost = 1.405MDA operation</td><td>0.136 $</td></tr>
<tr><td>V. Total cost
Cost of an operation = cost of raw materials + cost of electricity + cost of manpower = $0.000025 + 0.0407 + 0.133309
Operation cost = 1.823 MAD
Cost of an operation = 0.177</td><td>0.177 $</td></tr>
</table>

Note the currency conversion used for the entire calculation is $1 = 10.31 MAD

at 40°C for both adsorbents, whereas at 40°C the Freundlich model was best suited to the experimental data for the adsorption of phenol on RRC and TRC. The thermodynamic study showed that the adsorption of phenol is spontaneous, physisorbed and endothermic on RRC and TRC. FTIR and XRD analyzes of the adsorbents after adsorption show that the phenol was adsorbed and penetrated into the inter-layer space resulting in an expansion of the latter.

References

[1] B. Huang, C. Lei, C. Wei, G. Zeng, Chlorinated volatile organic compounds (Cl-VOCs) in environment — sources, potential human health impacts, and current remediation technologies, Environ. Int., 71 (2014) 118–138.

[2] S.M. Cordova-Rosa, R.I. Dams, E.V. Cordova-Rosa, M.R. Radetski, A.X.R. Corrêa, C.M. Radetski, Remediation of phenol-contaminated soil by a bacterial consortium and *Acinetobacter calcoaceticus* isolated from an industrial wastewater treatment plant, J. Hazard. Mater., 164 (2009) 61–66.

[3] K. Ikehata, M.G. El-Din, S.A. Snyder, Ozonation and advanced oxidation treatment of emerging organic pollutants in water and wastewater, Ozone Sci. Eng., 30 (2008) 21–26.

[4] D.W. Sundstrom, B.A. Weir, H.E. Klei, Destruction of aromatic pollutants by UV light catalyzed oxidation with hydrogen peroxide, Environ. Prog., 8 (1989) 6–11.

[5] L.G.C. Villegas, N. Mashhadi, M. Chen, D. Mukherjee, K.E. Taylor, N. Biswas, A short review of techniques for phenol removal from wastewater, Curr. Pollut. Rep., 2 (2016) 157–167.

[6] G. Busca, S. Berardinelli, C. Resini, L. Arrighi, Technologies for the removal of phenol from fluid streams: a short review of recent developments, J. Hazard. Mater., 160 (2008) 265–288.

[7] S. Mohammadi, A. Kargari, H. Sanaeepur, K. Abbassian, A. Najafi, E. Mofarrah, Phenol removal from industrial wastewaters: a short review, Desal. Water Treat., 53 (2015) 2215–2234.

[8] C.M. Santana, Z.S. Ferrera, M.E.T. Padrón, J.J.S. Rodríguez, Methodologies for the extraction of phenolic compounds from environmental samples: new approaches, Molecules, 14 (2009) 298–320.

[9] S.A. Boyd, G. Sheng, B.J. Teppen, C.T. Johnston, Mechanisms for the adsorption of substituted nitrobenzenes by smectite clays, Environ. Sci. Technol., 35 (2001) 4227–4234.

[10] Z. Li, P.H. Chang, J.S. Jean, W.T. Jiang, C.J. Wang, Interaction between tetracycline and smectite in aqueous solution, J. Colloid Interface Sci., 341 (2010) 311–319.

[11] A. de Mello Ferreira Guimarães, V.S.T. Ciminelli, W.L. Vasconcelos, Smectite organofunctionalized with thiol groups for adsorption of heavy metal ions, Appl. Clay Sci., 42 (2009) 410–414.

[12] C. Rey, C. Combes, C. Drouet, H. Sfihi, A. Barroug, Physico-chemical properties of nanocrystalline apatites: implications for biominerals and biomaterials, Mater. Sci. Eng. C, 27 (2007) 198–205.

[13] E. Picard, H. Gauthier, J.F. Gérard, E. Espuche, Influence of the intercalated cations on the surface energy of montmorillonites: consequences for the morphology and gas barrier properties of polyethylene/montmorillonites nanocomposites, J. Colloid Interface Sci., 307 (2007) 364–376.

[14] C. Queffélec, M. Petit, P. Janvier, D.A. Knight, B. Bujoli, Surface modification using phosphonic acids and esters, Chem. Rev., 112 (2012) 3777–3807.

[15] D. Merinska, Z. Malac, M. Pospisil, Z. Weiss, M. Chmielova, P. Capkova, J. Simonik, Polymer/clay nanocomposites based on MMT/ODA intercalates, Compos. Interfaces, 9 (2002) 529–540.

[16] S.F.A. Shattar, N.A. Zakaria, K.Y. Foo, Feasibility of montmorillonite-assisted adsorption process for the effective treatment of organo-pesticides, Desal. Water Treat., 57 (2016) 13645–13677.

[17] V.C. Sanchez, A. Jachak, R.H. Hurt, A.B. Kane, Biological interactions of graphene-family nanomaterials: An interdisciplinary review, Chem. Res. Toxicol., 25 (2012) 15–34.

[18] B.F. Sels, D.E. De Vos, P.A. Jacobs, Hydrotalcite-like anionic clays in catalytic organic reactions, Catal. Rev. Sci. Eng., 43 (2001) 443–488.

[19] A. Dümig, W. Häusler, M. Steffens, I. Kögel-Knabner, Clay fractions from a soil chronosequence after glacier retreat reveal the initial evolution of organo-mineral associations, Geochim. Cosmochim. Acta, 85 (2012) 1–18.

[20] J.A. Cecilia, C. García-Sancho, E. Vilarrasa-García, J. Jiménez-Jiménez, E. Rodriguez-Castellón, Synthesis, characterization, uses and applications of porous clays heterostructures: a review, Chem. Rec., 18 (2018) 1085–1104.

[21] S.A. Hadigheh, R.J. Gravina, S.T. Smith, Effect of acid attack on FRP-to-concrete bonded interfaces, Constr. Build. Mater., 152 (2017) 285–303.

[22] P. Komadel, J. Madejová, Acid Activation of Clay Minerals, 2nd ed., Institute of Inorganic Chemistry, Slovak Academy of Sciences, Bratislava, Slovakia, 2013. Available at: https://doi.org/10.1016/B978-0-08-098258-8.00013-4

[23] P. Komadel, Acid activated clays: materials in continuous demand, Appl. Clay Sci., 131 (2016) 84–99.

[24] F. Hussin, M.K. Aroua, W.M.A.W. Daud, Textural characteristics, surface chemistry and activation of bleaching earth: a review, Chem. Eng. J., 170 (2011) 90–106.

[25] F.R. Valenzuela Díaz, P. de Souza Santos, Studies on the acid activation of Brazilian smectitic clays, Quim. Nova, 24 (2001) 345–353.

[26] A. Gil, L.M. Gandía, M.A. Vicente, Recent advances in the synthesis and catalytic applications of pillared clays, Catal. Rev. Sci. Eng., 42 (2000) 145–212.

[27] H. Zhao, C.H. Zhou, L.M. Wu, J.Y. Lou, N. Li, H.M. Yang, D.S. Tong, W.H. Yu, Catalytic dehydration of glycerol to acrolein over sulfuric acid-activated montmorillonite catalysts, Appl. Clay Sci., 74 (2013) 154–162.

[28] C. Breen, R. Watson, J. Madejová, P. Komadel, Z. Klapyta, Acid-activated organoclays: preparation, characterization and catalytic activity of acid-treated tetraalkylammonium-exchanged smectites, Langmuir, 13 (1997) 6473–6479.

[29] R. Mokaya, W. Jones, Pillared clays and pillared acid-activated clays: a comparative-study of physical, acidic, and catalytic properties, J. Catal., 153 (1995) 76–85.

[30] M. Lenarda, L. Storaro, A. Talon, E. Moretti, P. Riello, Solid acid catalysts from clays: preparation of mesoporous catalysts by chemical activation of metakaolin under acid conditions, J. Colloid Interface Sci., 311 (2007) 537–543.

[31] P. Komadel, J. Madejová, Chapter 7.1 Acid Activation of Clay Minerals, Developments in Clay Science, Vol. 1, Institute of Inorganic Chemistry, Slovak Academy of Sciences, SK-845 36 Bratislava, Slovakia, 2006, pp. 263–287. Available at: https://doi.org/10.1016/S1572-4352(05)01008-1

[32] Z.P. Zhang, M.Z. Rong, M.Q. Zhang, Polymer engineering based on reversible covalent chemistry: a promising innovative pathway towards new materials and new functionalities, Prog. Polym. Sci., 80 (2018) 39–93.

[33] M. Shamzhy, M. Opanasenko, P. Concepción, A. Martínez, New trends in tailoring active sites in zeolite-based catalysts, Chem. Soc. Rev., 48 (2019) 1095–1149.

[34] R. Raj, Fundamental research in structural ceramics for service near 2,000°C, J. Am. Ceram. Soc., 76 (1993) 2147–2174.

[35] H. Su, W. Zhou, Mechanism of accelerated dissolution of mineral crystals by cavitation erosion, Acta Geochim., 39 (2020) 11–42.

[36] A. Mandal, B.B. Dey, S.K. Das, Thermodynamics, kinetics, and isotherms for phenol removal from wastewater using red mud, Water Pract. Technol., 15 (2020) 705–722.

[37] N. Bar, A. Mandal, S.K. Das, A Machine Learning Technique for the Study of Adsorption of Phenol Using Solid Waste, S. Mukhopadhyay, S. Sarkar, J.K. Mandal, S. Roy, Eds., AI to Improve e-Governance and Eminence of Life. Studies in Big Data, Vol. 130, Springer, Singapore, 2023. Available at: https://doi.org/10.1007/978-981-99-4677-8_7

[38] D. Aran, A. Maul, J.F. Masfaraud, A spectrophotometric measurement of soil cation exchange capacity based on cobaltihexamine chloride absorbance, C.R. Geosci., 340 (2008) 865–871.

[39] H. Moussout, H. Ahlafi, M. Aazza, H. Maghat, Critical of linear and non-linear equations of pseudo-first-order and pseudo-second-order kinetic models, Karbala Int. J. Mod. Sci., 4 (2018) 244–254.
[40] Y.S. Ho, G. McKay, Modèle de pseudo-second-order pour les processus de sorption, Processus Biochimie., 34 (1999) 451–465.
[41] M. Aazza, H. Ahlafi, H. Moussout, H. Maghat, Adsorption of metha-nitrophenol onto alumina and HDTMA modified alumina: kinetic, isotherm and mechanism investigations, J. Mol. Liq., 268 (2018) 587–597.
[42] M.S. Barrios, L.V.F. González, M.A.V. Rodríguez, J.M.M. Pozas, Acid activation of a palygorskite with HCl: development of physico-chemical, textural and surface properties, Appl. Clay Sci., 10 (1995) 247–258.
[43] S. Saagari, D. Anusha, L. Priyanka, N. Sailaja, Data warehousing, data mining, OLAP and OLTP technologies are indispensable elements to support decision-making process in industrial world, Int. J. Innovation Technol. Explor. Eng., 5 (2015) 1–7.
[44] J.T. Kloprogge, E. Mahmutagic, R.L. Frost, Mid-infrared and infrared emission spectroscopy of Cu-exchanged montmorillonite, J. Colloid Interface Sci., 296 (2006) 640–646.
[45] J. Madejová, FTIR techniques in clay mineral studies, Vib. Spectrosc., 31 (2003) 1–10.
[46] W. Trabelsi, A. Tlili, Phosphoric acid purification through different raw and activated clay materials (Southern Tunisia), J. Afr. Earth Sci., 129 (2017) 647–658.
[47] H. Ouallal, M. Azrour, M. Messaoudi, H. Moussout, L. Messaoudi, N. Tijani, Incorporation effect of olive pomace on the properties of tubular membranes, J. Environ. Chem. Eng., 8 (2020) 103668, doi: 10.1016/j.jece.2020.103668.
[48] D. Ovadyahu, S. Yariv, I. Lapides, Mechanochemical adsorption of phenol by tot swelling clay minerals I. Thermo-IR-spectroscopy and X-ray study, J. Therm. Anal., 51 (1998) 415–430.
[49] S. Saltzman, S. Yariv, Infrared study of the sorption of phenol and p-nitrophenol by montmorillonite, Soil Sci. Soc. Am. J., 39 (1975) 474–479.
[50] Y. Bulut, H. Aydin, A kinetics and thermodynamics study of methylene blue adsorption on wheat shells, Desalination, 194 (2006) 259–267.
[51] A.K. Jain, Suhas, A. Bhatnagar, Methylphenols removal from water by low-cost adsorbents, J. Colloid Interface Sci., 251 (2002) 39–45.
[52] B.K. Singh, N.S. Rawat, Comparative sorption equilibrium studies of toxic phenols on flyash and impregnated flyash, J. Chem. Technol. Biotechnol., 61 (1994) 307–317.
[53] B.K. Singh, P.S. Nayak, Sorption equilibrium studies of toxic nitro-substituted phenols on fly ash, Adsorpt. Sci. Technol., 22 (2004) 295–310.
[54] B.H. Hameed, Equilibrium and kinetics studies of 2,4,6-trichlorophenol adsorption onto activated clay, Colloids Surf., A, 307 (2007) 45–52.
[55] R. Rostamian, M. Najafi, A.A. Rafati, Synthesis and characterization of thiol-functionalized silica nano hollow sphere as a novel adsorbent for removal of poisonous heavy metal ions from water: kinetics, isotherms and error analysis, Chem. Eng. J., 171 (2011) 1004–1011.
[56] B. Özkaya, Adsorption and desorption of phenol on activated carbon and a comparison of isotherm models, J. Hazard. Mater., 129 (2006) 158–163.
[57] E. Bazrafshan, P. Amirian, A.H. Mahvi, A. Ansari-Moghaddam, Application of adsorption process for phenolic compounds removal from aqueous environments: a systematic review, Global Nest J., 18 (2016) 146–163.
[58] E. Eren, B. Afsin, Removal of basic dye using raw and acid activated bentonite samples, J. Hazard. Mater., 166 (2009) 830–835.
[59] I. Poljanšek, M. Krajnc, Characterization of phenol-formaldehyde prepolymer resins by in line FTIR spectroscopy, Acta Chim. Slov., 52 (2005) 238–244.
[60] R. Liu, R.L. Frost, W.N. Martens, Near infrared and mid infrared investigations of adsorbed phenol on HDTMAB organoclays, Mater. Chem. Phys., 113 (2009) 707–713.
[61] H. Ouallal, Y. Dehmani, H. Moussout, L. Messaoudi, M. Azrour, Kinetic, isotherm and mechanism investigations of the removal of phenols from water by raw and calcined clays, Heliyon, 5 (2019) e01616, doi: 10.1016/j.heliyon.2019.e01616.
[62] A. Mandal, P. Mukhopadhyay, S.K. Das, Adsorptive removal of phenol from wastewater using guava tree bark, Environ. Sci. Pollut. Res., 27 (2020) 23937–23949.
[63] A. Mandal, P. Mukhopadhyay, S.K. Das, Efficiency analysis of rice husk as adsorbent for removal of phenol from wastewater, J. Environ. Anal. Toxicol., 9 (2019) 605–612.
[64] A. Mandal, P. Mukhopadhyay, S.K. Das, The study of adsorption efficiency of rice husk ash for removal of phenol from wastewater with low initial phenol concentration, SN Appl. Sci., 1 (2019) 192, doi: 10.1007/s42452-019-0203-3.
[65] A. Das, N. Bar, S.K. Das, Adsorptive removal of Pb(II) ion on *Arachis hypogaea's* shell: batch experiments, statistical, and GA modeling, Int. J. Environ. Sci. Technol., 20 (2022) 537–550.
[66] S. Bhattacharya, N. Bar, B. Rajbansi, S.K. Das, Synthesis of chitosan-*n*TiO_2 nanocomposite, application in adsorptive removal of Cu(II)—adsorption and desorption study, mechanism, scale-up design, statistical, and genetic algorithm modeling, Appl. Organomet. Chem., 37 (2023) e7094, doi: 10.1002/aoc.7094.